AGU100 ADVANCING EARTH AND SPACE SCIENCE

JGR Solid Earth

RESEARCH ARTICLE
10.1029/2019JB018128

Special Section:
Magnetism in the Geosciences - Advances and Perspectives

Key Points:
- We found inverse fabrics in pelagic clay from the western North Pacific with high concentration of magnetofossils
- Magnetofossils can control the bulk susceptibility of pelagic clay
- Magnetofossils in the studied pelagic clay exhibit weaker foliation than terrigenous minerals

Correspondence to:
Y. Usui,
yoichi@jamstec.go.jp

Citation:
Usui, Y., Yamazaki, T., Oka, T., & Kumagai, Y. (2019). Inverse magnetic susceptibility fabrics in pelagic sediment: Implications for magnetofossil abundance and alignment. *Journal of Geophysical Research: Solid Earth*, *124*, 10,672–10,686. https://doi.org/10.1029/2019JB018128

Received 30 MAY 2019
Accepted 17 OCT 2019
Accepted article online 31 OCT 2019
Published online 8 NOV 2019

Inverse Magnetic Susceptibility Fabrics in Pelagic Sediment: Implications for Magnetofossil Abundance and Alignment

Yoichi Usui[1], Toshitsugu Yamazaki[2], Toshitaka Oka[3,4], and Yuho Kumagai[5]

[1]Volcanoes and Earth's Interior Research Center, Research Institute of Marine Geodynamics, Japan Agency for Marine-Earth Science and Technology (JAMSTEC), Yokosuka, Japan, [2]Atmosphere and Ocean Research Institute, The University of Tokyo, Kashiwa, Japan, [3]Institute for Excellence in Higher Education, Tohoku University, Sendai, Japan, [4]Now at Nuclear Science and Engineering Center, Japan Atomic Energy Agency, Naka-gun, Japan, [5]Department of Earth Science, Tohoku University, Sendai, Japan

Abstract Single-domain magnetite particles exhibit minimum susceptibility along their elongation, resulting in so-called inverse fabric of the anisotropy of magnetic susceptibility (AMS). We report the discovery of inverse AMS fabrics from pelagic clay recovered by a ~ 12 m long piston core from the western North Pacific. A previous study identified fossil single-domain magnetite produced by magnetotactic bacteria (magnetofossils) as the dominant ferrimagnetic mineral in the sediment. The inverse AMS fabrics were found in a ~ 2 m zone. The ~ 6 and ~ 4 m of sediment above and below this zone showed normal, horizontal AMS fabrics. Rock magnetic data and ferromagnetic resonance spectroscopy indicated that magnetofossils account for most of the mean susceptibility regardless of normal or inverse AMS. This was explained by the mixing models where the inverse fabric from magnetofossils is nearly balanced by the normal fabrics of terrigenous minerals. The corrected degree of AMS carried by magnetofossils in the sediment was estimated to be ~ 1.01, which is comparable to that of typical pelagic sediment at shallow depth. On the other hand, terrigenous minerals in the sediment were estimated to have higher degree of anisotropy, possibly reflecting burial and subsequent erosion of > 80 m of sediment, which was also suggested by a subbottom acoustic stratigraphy. This suggests that inverse AMS fabrics due to magnetofossils may be widespread in pelagic clay without strong compaction.

1. Introduction

The anisotropy of low field magnetic susceptibility (AMS) of sediment has been investigated to characterize fabric produced by compaction, deformation, or paleocurrent (e.g., Jackson & Tauxe, 1991; Kanamatsu et al., 2012; Kawamura & Ogawa, 2004; Kon et al., 2017; Maffione & Morris, 2017; MacDonald & Ellwood, 1987; Parés et al., 2007; Schwehr et al., 2006). Most of the common magnetic minerals show maximum magnetic susceptibility along their long dimension (e.g., Tarling & Hrouda, 1993). Consequently, bulk AMS is usually concordant with macroscopic fabrics such as a bedding plane. Such AMS fabric is termed normal fabric; the normal fabric is the underlying assumption to interpret AMS. In contrast, elongated single-domain (SD) magnetite and maghemite exhibit the minimum susceptibility along the elongation, because the elongation direction is the magnetic easy axis (Potter & Stephenson, 1988); remanence is along the easy direction under zero field, so a weak external field induces hardly any additional magnetization along that direction. Thus, the AMS of a sample with abundant SD magnetite would be perpendicular to macroscopic fabrics, resulting in so-called inverse fabric (Rochette et al., 1992). This effect is not present for remanence anisotropy (e.g., Jackson, 1991). Even if the abundance of SD magnetite is insufficient to produce bulk inverse fabrics, the inverse component could reduce the bulk anisotropy intensity (Ferré, 2002; Rochette et al., 1992). Therefore, detecting the inverse contribution of SD magnetite is an important step in AMS studies. Overall, studies have shown that inverse AMS fabrics due to SD magnetite are not common. This has been explained as due to overwhelming contribution of coexisting larger multidomain grains or smaller superparamagnetic grains which exhibit normal fabrics (Hrouda & Ježek, 2017; Lanci & Zanella, 2016).

One of the special situations where SD magnetite is selectively produced is through biomineralization. Magnetotactic bacteria produce magnetite and greigite crystals with precisely controlled morphology and

arrangement called magnetosomes (e.g., Bazylinski & Frankel, 2004). Magnetosomes can be preserved in sediment as fossils (magnetofossils) of noninteracting SD particles (Kirschvink & Chang, 1984; Petersen et al., 1986). Therefore, magnetofossils in sediment and sedimentary rocks are expected to show inverse AMS fabrics. Recent studies revealed that magnetofossils are widespread in sediment (e.g., Just et al., 2012; Roberts et al., 2012, 2013; Yamazaki, 2012; Yamazaki & Shimono, 2013). Nonetheless, to our knowledge, a magnetic fabric attributed to magnetofossils has not been reported from natural sediment. This may be due to the insignificant abundance of magnetofossils in terms of susceptibility. Alternatively, because magnetofossils are genetically different from detrital ferrimagnetic or paramagnetic minerals, their macroscopic fabrics may be distinct. An experimental study (Mao et al., 2014) suggested that the alignment of magnetosomes within sediment due to the geomagnetic field may be minor (<1%). On the other hand, the fabric development of magnetofossils due to deformation has not been studied; if magnetofossils have weaker preferred orientation than the other minerals, their effect on bulk anisotropy may be limited.

Magnetic fabrics of magnetofossils are also expected to be important for environmental magnetism and paleomagnetism. The abundance and morphology of magnetofossils was proposed as a paleoenvironmental proxy (e.g., Chang et al., 2018; Hesse, 1994; Kopp et al., 2007; Roberts et al., 2011; Usui et al., 2017; Yamazaki, 2012; Yamazaki & Kawahata, 1998; Yamazaki & Shimono, 2013; Yamazaki et al., 2019). Various rock magnetic methods have been applied to quantify it including the ratio of susceptibility of anhysteretic remanence over saturation isothermal remanence (kARM/SIRM), first-order reversal curves (FORCs), and ferromagnetic resonance (FMR) spectroscopy (e.g., Egli et al., 2010; Li et al., 2012; Weiss et al., 2004). One of the key concepts in those methods is that magnetofossils exhibit special characteristics such as narrow coercivity distribution, minimal magnetostatic interaction, and strong chain scale anisotropy, so that their contribution can be unmixed from background (Gehring et al., 2011; Heslop et al., 2013; Lascu et al., 2015). Because inverse AMS fabrics are rare in sediment, the amount of magnetofossils may also be obtained through unmixing of AMS fabrics. The alignments of magnetosomes within sediment are likely to be controlled by the direction and intensity of the external magnetic field (Mao et al., 2014), so by quantifying the fabric of magnetofossils, one may recover some paleomagnetic information.

Usui et al. (2017) reported high abundance of magnetofossils in pelagic red clay from the western North Pacific, confirming the earlier reports that red clay often contains abundant magnetofossils (Shimono & Yamazaki, 2016; Yamazaki & Shimono, 2013). Particularly, they estimated large abundance variation of magnetofossils. This offers a chance to detect possible contribution of magnetofossils to AMS. Here we report AMS and rock magnetic data from this sediment. By correlating AMS and rock magnetic data, we discuss the abundance and alignment of magnetofossils, as well as the fabric of background terrigenous minerals.

2. Theory

AMS can be described by the orientation and magnitude of three principal susceptibility $K_1 \geq K_2 \geq K_3$ of the susceptibility tensor. The fabric can be conveniently characterized by a shape parameter T_j and an anisotropy degree P_j defined as

$$T_j = \frac{2\eta_2 - \eta_1 - \eta_3}{\eta_1 - \eta_3} \tag{1}$$

$$P_j = \exp\sqrt{2[(\eta_1 - \eta_m)^2 + (\eta_2 - \eta_m)^2 + (\eta_3 - \eta_m)^2]} \tag{2}$$

where $\eta_i = \ln K_i \quad (i = 1, 2, 3)$ and $\eta_m = (\eta_1 + \eta_2 + \eta_3)/3$ (Jelinek, 1981). Usually, sediment has only moderate interparticle magnetostatic interaction; in this case, susceptibility of subpopulations within a sample can be simply summed. Moreover, when AMS of the subpopulations (subfabrics) is coaxial, as is expected for undeformed sediment, the bulk AMS can be obtained by adding up collinear principal susceptibilities of the subfabrics. When we consider normalized susceptibility $k_i = K_i/K_m$ where K_m is the mean susceptibility $(K_1 + K_2 + K_3)/3$, the AMS resulting from a combination of two subfabrics $k^{(1)}$ and $k^{(2)}$ is given by

$$k_j = pk_j^{(1)} + (1 - p)k_j^{(2)} \tag{3}$$

where $j = x, y, z$ is the external coordinate and p is the mixing ratio of $k^{(1)}$, that is, $p = K_m^{(1)}/(K_m^{(1)} + K_m^{(2)})$ (Henry & Daly, 1983).

A particular interest is in the relative contributions between paramagnetic minerals which is expected to show a normal fabric and ferrimagnetic minerals which may include an inverse fabric. The magnetization of ferrimagnetic minerals, especially of magnetite, saturates at moderately high field (on the order of 100 mT for magnetite), resulting in zero susceptibility. On the other hand, susceptibility of paramagnetic minerals is practically independent of the field (e.g., Dunlop & Özdemir, 1997). Therefore, susceptibility measured at high field can be used to estimate the paramagnetic susceptibility.

The contribution of SD magnetite to bulk susceptibility can be increased by not only increasing abundance but also increasing grain susceptibility (volume normalized mean susceptibility of a single grain) of SD magnetite. Grain susceptibility is related to grain anisotropy. For uniaxial SD grains, grain susceptibility can be approximated using equilibrium magnetization of the Stoner-Wohlfarth particles under a small applied field as

$$\frac{K_m}{M_s} = \frac{\mu_0 M_s}{3K_u} \tag{4}$$

where μ_0 is the permeability of vacuum, M_s the saturation magnetization, and K_u the uniaxial anisotropy constant (e.g., Lanci, 2010). A chain of magnetosomes can be effectively considered as a single SD grain dominated by uniaxial anisotropy with an additional contribution from crystallographic anisotropy (Charilaou, 2017; Charilaou et al., 2011). The intensities of both anisotropies can be estimated using FMR. For magnetite magnetosomes, the resonance field B_{res} has been modeled using the first-order anisotropy constants K_u (uniaxial anisotropy) and K_c (magnetocrystalline anisotropy), M_s, and the crystallographic orientation of crystals with respect to the chain (Charilaou, 2017; Charilaou et al., 2011, 2015). K_u reflects interparticle magnetostatic interaction within the chain as well as grain elongation. K_c reflects the cubic magnetocrystalline anisotropy. For perfect magnetite $K_c = -13.5$ kJ/m^3 (Dunlop & Özdemir, 1997), however, from some sediment and magnetosomes, lower values have been inferred and interpreted as due to maghemitization (Fischer et al., 2007) or intracrystal inhomogeneity (Charilaou, 2017). The crystallographic orientation may be either that the [111] directions (the magnetic easy axes) parallel to the chain or that the [100] directions parallel to the chain; the latter have been observed for some bullet-shaped magnetosomes (Lefèvre et al., 2011; Pósfai et al., 2006). Conventionally, these parameters have been combined as

$$B_{\mathrm{uni}} = 2K_u/M_s \tag{5}$$

$$B_{\mathrm{cub}} = K_c/M_s \tag{6}$$

(Charilaou et al., 2011). From B_{res}, the microwave absorption can be calculated with a line broadening function $f(B; B_{\mathrm{res}})$. The typical form of $f(B)$ is a Lorentzian, which can be characterized by another parameter ΔB as

$$f(B; B_{\mathrm{res}}, \Delta B) = \frac{\Delta B/2}{\pi[(B - B_{\mathrm{res}})^2 + (\Delta B/2)^2]} \tag{7}$$

Simulated FMR spectra are then obtained as the derivative of $f(B)$. By fitting FMR spectra using simulated spectra of magnetosomes and a symmetric component coming from near-isotropic particles other than magnetosomes, one can estimate B_{uni} and B_{cub} of magnetofossils in sediment (Chang et al., 2014; Gehring et al., 2011) that in turn give the equilibrium magnetization vector to estimate grain susceptibility of magnetofossils.

3. Materials

We studied a piston core PC12 recovered during the cruise MR15-E01_Leg2 around Minamitorishima Island in the western North Pacific (Usui et al., 2017). This core was ~ 12 m of brown to dark brown clay. The core liners were made of polycarbonate, which was annealed before the cruise to minimize the deformation of the liners after splitting. Usui et al. (2017) conducted a rock magnetic and microscopic study on the core. The results showed abundant magnetofossils especially below a possible hiatus at ~ 5.3 m, characterized by high kARM/SIRM and pronounced central ridge in the FORC diagrams. On the basis of the linear unmixing of isothermal remanent magnetization curves and microscopic observations, the proportion of

elongated magnetofossils to equant ones and the total magnetofossil abundance are estimated to be highest at around 7 m.

Nakamura et al. (2016) reported acoustic data around Minamitorishima Island. They showed that the sediment in the region consists of two acoustic facies: underlying transparent facies and overlying layered facies. Interestingly, the thickness of the layered facies varies significantly from 0 to >40 m, suggesting local hiatus or erosion. The core PC12 was from a site without the layered facies (Nakamura et al., 2016; Usui et al., 2017).

4. Methods

We measured AMS and the anisotropy of anhysteretic remanence (AARM) to detect possible inverse AMS fabrics. Sediment samples were obtained using standard 7 cm^3 plastic cubes from the archive half. Samples were not taken between 3.20 and 3.97 m in core depth due to core disturbance (Usui et al., 2017). We used the following right-handed core coordinate system: $+x$ points normal outward from the core split surface of the archive half and $+z$ points downward. AMS was measured using a Kappabridge KLY-4 (AGICO) with software SUFAR.

AARM were measured on selected cube specimens. ARMs were imparted using an alternating field (AF) demagnetizer DEM95 (Natsuhara Giken) with a peak AF of 100 mT and a direct-current field of 0.07 mT. Decay rate was set as "60" in the demagnetizer. ARMs were imparted along nine directions (Girdler, 1961). Before each ARM acquisition, samples were AF demagnetized at 150 mT with two axes tumbling. ARM vectors were fitted by a second-rank tensor using least squares using in-house software.

To estimate the abundance of magnetofossils, we analyzed paramagnetic susceptibility (K_p), FORCs, and FMR on selected samples. Initial susceptibility (K_{vsm}) and susceptibility at high field K_h were measured on a vibration sample magnetometer (VSM) Model 3902 (Princeton Measurements) for $\sim$ 1 cm^3 subsamples taken from the 7 cm^3 cubes. Before measurements, samples were AF demagnetized at 150 mT using the AF demagnetizer. K_h was calculated by simple linear fits for hysteresis loops measured with maximum field of 1 T. Data for field magnitude $||B|| > 0.7$ T were fitted with a line, and the slope was taken as K_h. Because the volume of the subsamples used for K_h and K_{vsm} measurements were not accurately measured, we used the ratio K_h/K_{vsm} to estimate the ratio of paramagnetic susceptibility to initial susceptibility. Then the paramagnetic susceptibility K_p was calculated as $(K_h/K_{\mathrm{vsm}}) \times K_m$. The ferrimagnetic susceptibility K_f was calculated as $K_m - K_p$.

FORCs were measured also using the VSM. We used the saturation field of 500 mT, the maximum reversal field of −97 mT, and field steps of 0.5 mT. FORCs were analyzed using software VARIORC ver. 4.01 (Egli, 2013). In particular, we isolated and quantified the contribution of the central ridge following the method of Egli et al. (2010), where the vertical profiles of the central ridge and the background distribution were fitted with model functions. We used the ratio of the integral of the central ridge relative to the integral of the entire FORC distribution, M_{CR}/M_{irs}, to quantify the contribution of the central ridge. This ratio ranges from 0 for pure multidomain grains to 1 for pure noninteracting SD grains. The detailed analyses parameters can be downloaded from a repository (see data availability in the Acknowledgments section).

FMR spectra were obtained using a JES-RE2X ESR spectrometer (JEOL) at the Department of Chemistry, Tohoku University. The frequency of microwave was $\sim$ 9.4 GHz (X-band), and the power was 1 mW. The range of the applied magnetic field was 0–800 mT. The spectra were compared visually with simulated spectra for randomly oriented magnetosomes (Charilaou, 2017; Charilaou et al., 2011, 2015) through a grid search for B_{uni} and B_{cub} at 1 mT resolution.

5. Results

5.1. Magnetic Anisotropies

Majority of the samples revealed normal AMS fabrics concordant with horizontal bedding, as indicated by near-vertical K_3 directions (Figures 1a and 1d). The interval from $\sim$ 2 to 3.2 m shows some deviation and scatter in the K_3 directions. We consider this as due to the core disturbance, which was obvious at 3.2–3.97 m. K_1 and K_2 axes distributed almost randomly in the horizontal plane with only very weak preference of the K_1 declination toward ~280° in core coordinates, resulting in $T_j \sim 1$ (Figure 1e). However, around 6.7–8.6 m, AMS revealed inverse fabrics with horizontal K_3 (Figures 1b–1d). T_j was close to −1 in

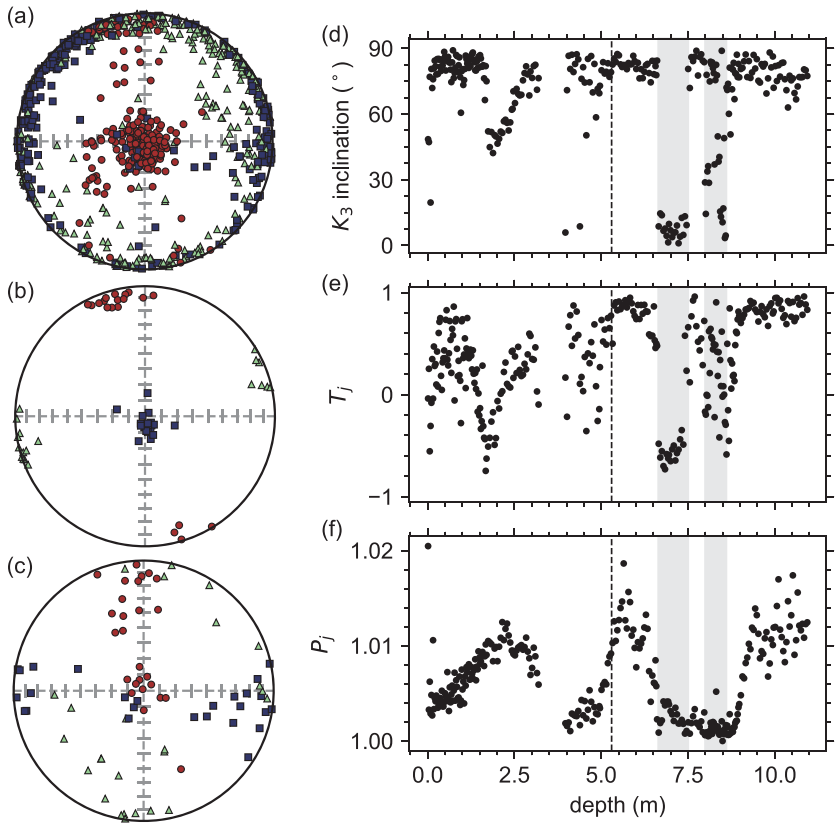

Figure 1. (a–c) Equal area projection of the principal AMS axes directions in core coordinates. Blue squares are K_1, green triangles are K_2, and red circles are K_3. Panel (a) displays all data, (b) 6.65–7.5 m, and (c) 8–8.6 m. (d–f) Depth profile of AMS parameters. Shaded areas indicate the intervals with the inverse fabrics (6.65–7 and 8–8.6 m). Vertical dashed lines indicate the position of possible hiatus (Usui et al., 2017).

this interval. The degree of anisotropy is generally low, $P_j < 1.02$ (Figure 1f). The anisotropy was particularly low around the interval with the inverse AMS; nonetheless, the K_3 axes showed preferred orientation at ~0° (Figures 1b and 1c).

The inverse fabrics were confirmed by AARM which showed only normal fabrics, indicating that core disturbance as a cause for the discordant AMS can be ruled out (Figure 2). The maximum AARM axes showed a preferred direction similar to K_3 of the samples with the inverse AMS.

K_m was on the order of 10^{-3} SI, indicating dominant contribution of ferrimagnetic minerals (Figure 3). Overall, the profile of K_m matched with SIRM except for a large peak at around 6 m in K_m, supporting that the ferrimagnetic minerals controlled K_m.

5.2. Ferrimagnetic and Paramagnetic Susceptibility

K_h/K_{vsm} ranged from 0.04 to 0.14, also showing the dominant contribution of ferrimagnetic minerals compared to the paramagnetic minerals (Figure 4). K_f showed good correlation with SIRM throughout the core (Figure 4). K_p was smaller around the interval with the inverse AMS (Figure 4e).

5.3. FORCs

Usui et al. (2017) had already reported the FORC diagrams from this core. They showed clear central ridge, especially below ~ 5.5 m. The depth profile of the ratio M_{CR}/M_{irs} correlated very well with kARM/SIRM (Figure 5), supporting the use of kARM/SIRM to detect noninteracting SD particles (Li et al., 2012). The M_{CR}/M_{irs} was stable at ~0.62–0.69 below ~ 5.5 m, including the intervals with inverse AMS fabrics. The values did not correlate with SIRM or K_m (Figure 3).

5.4. FMR

Below ~ 5.5 m, FMR spectra showed strong asymmetry (Figure 6), which is suggestive of the presence of magnetosomes (Weiss et al., 2004; Kopp et al., 2006; Charilau et al., 2011). This is consistent with the high

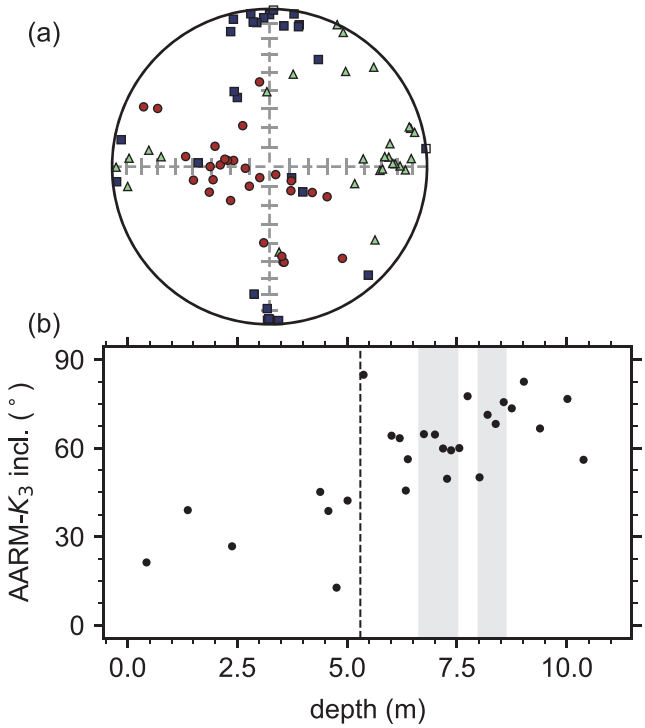

Figure 2. (a) Equal area projection of the principal AARM axes directions in core coordinates. Blue squares are maximum, green triangles are intermediate, and red circles are minimum direction. (b) Depth profile of the inclindation of the minimum AARM axis. Shaded areas indicate the intervals with the inverse AMS fabrics (6.65–7.5 and 8–8.6 m). Vertical dashed line indicates the position of possible hiatus.

kARM/SIRM and M_{CR}/M_{irs} in this interval. The spectra also revealed peaks broadly similar to the intact magnetosomes from cultured magnetotactic bacteria (Kopp et al., 2006; Weiss et al., 2004). This is in contrast with a previous report of FMR spectra for pelagic clay from the Atlantic (Kopp et al., 2006), showing that at least some pelagic clay contains well preserved chains of magnetite. The first peaks of the spectra were at around 245 mT, which is higher field compared to the spectra obtained from cultured magnetotactic bacteria (Kopp et al., 2006; Weiss et al., 2004). The spectra shapes did not correlate directly with the AMS fabrics but with the morphology of magnetofossils. On the basis of the component analyses of isothermal remanence, Usui et al. (2017) estimated that the elongated magnetofossils are dominant between ~6.5 and 8 m. The FMR spectra for this interval were distinct; the peak around 400 mT was shifted toward higher field than the other samples (Figure 6).

We selected the samples from 5.69 and 7.13 m as the most representative of the equant and elongated magnetofossils, respectively. Reasonable fits with simulated spectra were found for the equant magnetofossils (5.69 m) with $B_{\mathrm{uni}} = 90 \pm 3$ mT, $B_{\mathrm{cub}} = -1^{+1}_{-2}$ mT, and $\Delta B = 60$ mT, together with the isotropic background with $B_{\mathrm{res}} = 320$ mT (Figure 7). We note that these B_{cub} are much lower than the value expected for magnetite (~ 23 mT). Maghemitization can partly account for this difference (Fischer et al., 2007), which should be pervasive in oxic red clay. However, pure maghemite still have $B_{\mathrm{cub}} = -12.2$ mT with $K_c = -4.65$ kJ/m^3 and $M_s = 380$ kA/m (Dunlop & Özdemir, 1997), and experimentally obtained FMR spectra of partly maghemitized magnetosomes showed B_{cub} similar to nonoxidized magnetosomes (Gehring et al., 2012). The low B_{cub} may reflect inhomogeneity of the field within single crysals (Charilaou, 2017) or chains. In this and following calculations, we consider that the magnetofossils were maghemitized, and $M_s = 380$ kA/m. The main aspects would not change if we use $M_s = 480$ kA/m (magnetite). For the elongated magnetofossils (7.13 m), reasonable fits were found using the model where the [100] directions are along the chain (Charilaou et al., 2015). The parameter ranges were $B_{\mathrm{uni}} = 104 \pm 3$ mT and $B_{\mathrm{cub}} = -5^{+2}_{-1}$ mT (Figure 7).

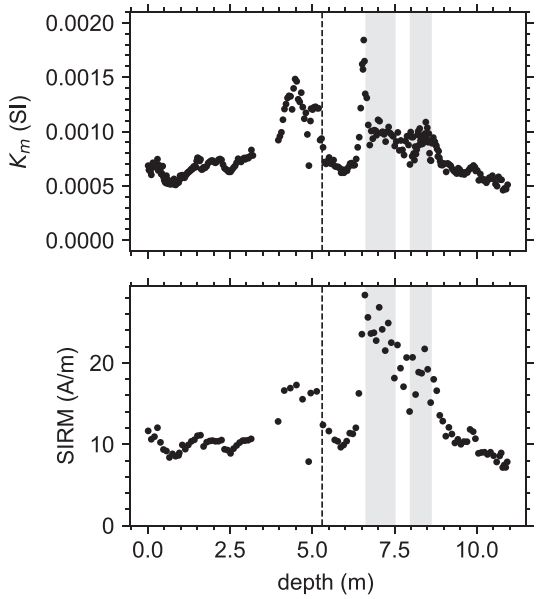

Figure 3. Depth profile of K_m and SIRM. Shaded areas indicate the intervals with inverse AMS fabric (6.65–7.5 and 8–8.6 m). SIRM data are from Usui et al. (2017). Vertical dashed lines indicate the position of the possible hiatus.

6. Discussion

The comparison between AMS and AARM indicated that the inverse AMS fabrics observed at around 7 m were due to SD magnetite. High K_m, close correlation between K_m and SIRM, and low K_h/K_{vsm} showed that ferrimagnetic minerals controlled K_m, while rock magnetic and microscopic data showed that magnetofossils were the main ferrimagnetic minerals (Usui et al., 2017). Thus, the variation of AMS is likely to reflect the abundance and alignment of magnetofossils. The inverse AMS was only observed at particular intervals.

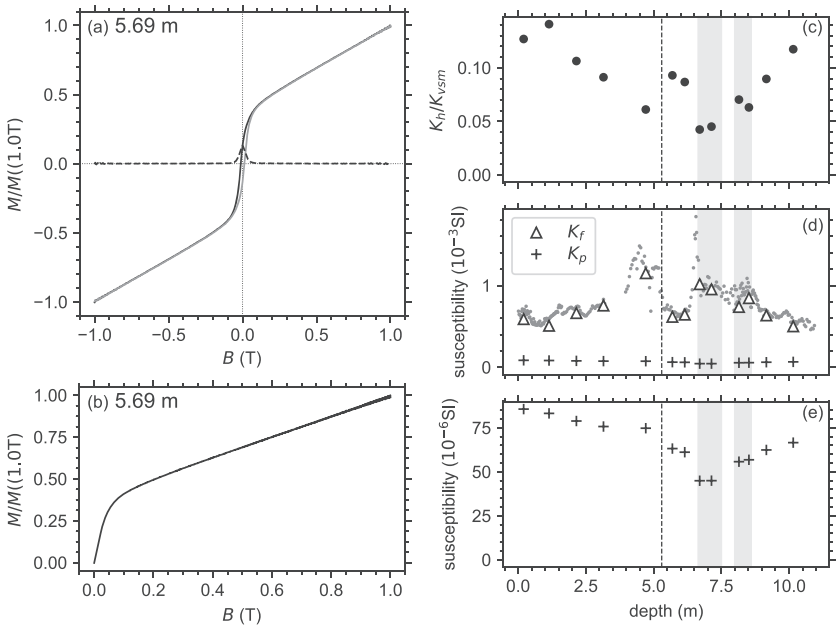

Figure 4. (a) Example of hysteresis loop. Dashed line represents remanent hysteresis (von Dobeneck, 1996). (b) Example of initial magnetization curve measurements. (c) Depth profile of K_h/K_{vsm}. (d, e) Depth profile of ferrimagnetic susceptibility K_f (open triangles) and paramagnetic susceptibility K_p (crosses). Small gray circles represent K_m. Shaded area indicate the intervals with the inverse AMS fabrics (6.65–7.5 and 8–8.6 m). Vertical dashed lines in (c–e) indicate the position of possible hiatus.

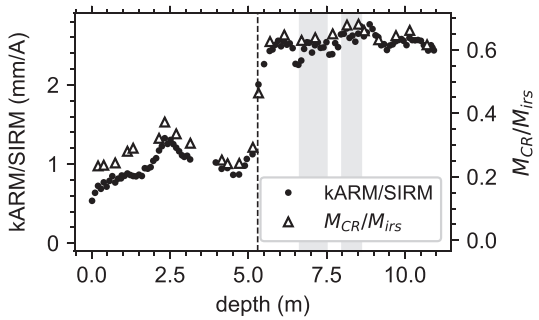

Figure 5. Depth profile of kARM/SIRM (black circles, left axis) and M_{CR}/M_{irs} (open triangles, right axis). Shaded area indicate the intervals with the inverse AMS fabrics (6.65–7.5 and 8–8.6 m). kARM/SIRM data are from Usui et al. (2017). A vertical dashed line indicates the position of the possible hiatus.

This implies that the magnetofossils have a limited contribution to the anisotropy, while they have a large contribution to K_m. We will examine this quantitatively using simple mixing models. In the sediment, we may consider three subfabrics of AMS: K^i an inverse fabric from magnetofossils, K^j a normal fabric from terrigenous ferrimagnetic minerals, and K^p from paramagnetic minerals. We will first examine the mixing of mean susceptibility and then consider the mixing of subfabrics to constrain the anisotropy.

The three-component mixing model for the mean susceptibility is

$$K_m^i = pK_m \tag{8}$$

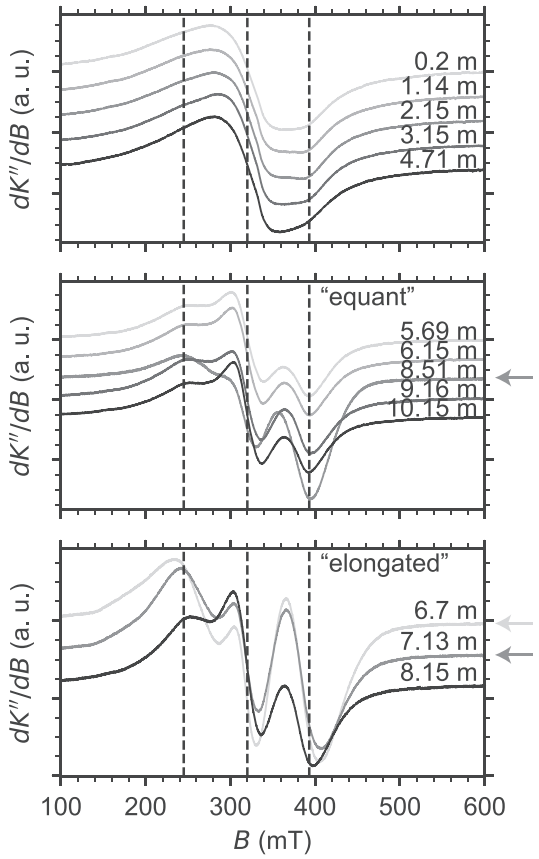

Figure 6. FMR spectra. (top) Samples above 5.5 m where kARM/SIRM are relatively low. (middle) Samples where the dominance of the equant magnetofossils was estimated. (bottom) Samples where the dominance of the elongated magnetofossils was estimated. Arrows on the right indicate the samples showing the inverse AMS fabric. Vertical dashed lines are eye guides at 245, 320, and 393 mT.

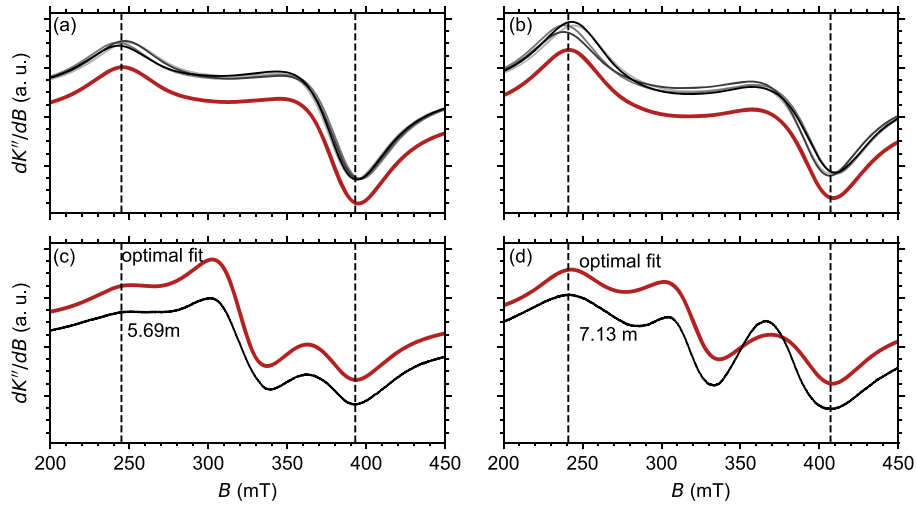

Figure 7. Fitting for the FMR spectra. (a) Simulated magnetofossil spectra for 5.69 m. The gray curves represent the calculations for the plausible range of the parameters ($B_{\mathrm{uni}} = 90 \pm 3$ mT and $B_{\mathrm{cub}} = -1^{+1}_{-2}$ mT), and the thick red curve represents the optimal case ($B_{\mathrm{uni}} = 90$ mT and $B_{\mathrm{cub}} = -1$ mT). (b) Simulated magnetofossil spectra for 7.13 m. The gray curves represent the calculations for the plausible range of the parameters ($B_{\mathrm{uni}} = 104 \pm 3$ mT and $B_{\mathrm{cub}} = -5^{+2}_{-1}$ mT), and the thick red curve represents the optimal case ($B_{\mathrm{uni}} = 104$ mT and $B_{\mathrm{cub}} = -5$ mT). (c) The optimal fit (red) calculated with the simulated spectra in (a) and an isotropic contribution and the observed spectra (black) for 5.69 m. (d) The optimal fit (red) calculated with the simulated spectra in (b) and an isotropic contribution and the observed spectra (black) for 7.13 m. Vertical dashed lines are eye guides at 245 and 393 mT (a, c) or at 241 and 407 mT (b, d).

$$K^j_m = qK_m \tag{9}$$

$$K^p_m = (1 - p - q)K_m \tag{10}$$

where p and q are the mixing ratio of K^i_m and K^j_m, respectively. Usui et al. (2017) showed that the magnetofossils account for $> 89\%$ of IRM below 5.5 m, so p is likely to be much larger than q. To get some bounds for p from the susceptibility, we introduce an assumption that the contribution of K^j relative to K^p is near constant, that is,

$$c \simeq q/(1 - p) \tag{11}$$

This is likely to be valid for pelagic clay with constant composition of terrigenous flux and a diagenetic condition. On the other hand, Usui et al. (2017) reported the presence of hiatus at around 5.3 m, and the concentration of terrigenous ferrimagnetic minerals per unit volume increased upcore from this depth. Therefore, we restrict our model to the sediment below 5.5 m. The validity of the relation (11) is also supported from the anisotropy, as discussed later. We have obtained the proportion of ferrimagnetic minerals $K_f/K_m = p + q$ through the VSM measurements, so p is only dependent on c:

$$p = (K_f/K_m - c)/(1 - c) \tag{12}$$

Figure 8 shows the variation of p and q for various c. For large c, $p/(p + q)$ exhibits large variation, which is not compatible with near constant kARM/SIRM and M_{CR}/M_{irs} (Figure 5). In this model, near constant $p/(p + q)$ were obtained for $c < 0.5$.

Small c would suppress the variation in p, which makes the transition to inverse AMS difficult. An alternative explanation to allow larger c and a contrast among p and kARM/SIRM or M_{CR}/M_{irs} may be due to grain susceptibility, but we argue that this effect is limited. Theoretically, the contribution of magnetofossils to bulk susceptibility can be enhanced by increasing grain susceptibility without increasing volume nor remanence of magnetofossils. Grain susceptibility of SD particles depends on particle-scale anisotropy, and anisotropy of magnetosomes depends on the shape, the crystallographic orientation, and the chain configuration of constituting crystals (Charilaou, 2017). The interval with inverse AMS fabrics also coincides with

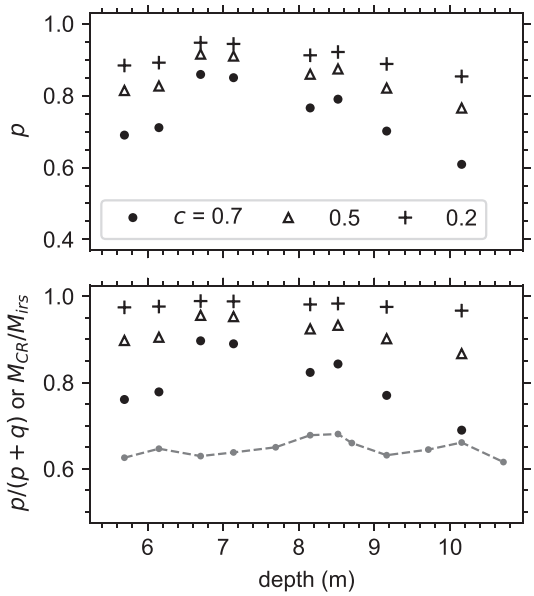

Figure 8. (top) Model calculations for the susceptibility mixing ratio of magnetosomes p. Black circles show the case with $c = 0.7$, open triangles $c = 0.5$, and crosses $c = 0.2$. (bottom) Comparison between the estimated magnetofossil contributions using susceptibility ($p/(p + q)$) and FORCs (M_{CR}/M_{irs}; gray circles connected by dashed line).

the peak abundance of the elongated magnetofossils (Usui et al., 2017). If the elongated magnetofossils have higher grain susceptibility, p can take higher values around 6.7–8.6 m as in the case $c > 0.5$ (Figure 8). We provide three lines of evidence argue against strong effect of grain susceptibility. First, we compare K_m and SIRM (Figure 9). If grain susceptibility increases, K_m / SIRM are expected to increase. However, the ratios do not change much, and at around 6.7–8.6 m, they exhibit minima rather than maxima.

A caveat is that K_m and SIRM include non-SD contributions, but at least there is no evidence for the enhanced grain susceptibility of magnetofossils in the interval. Second, the FMR spectra did not correlate with the AMS fabric. The sample from 8.51 m showed an inverse fabric, but the FMR spectra showed the peak positions similar to the sample from 5.69 m (Figure 6), which showed a normal fabric and interpreted as dominated by equant magnetofossils (Usui et al., 2017). Conversely, the sample from 8.15 m showed normal fabric, but the FMR spectra is similar to the samples from 6.7 and 7.13 m. Given that the FMR spectra possibly reflect the magnetofossil morphology, these results qualitatively argue against the controlling effect of the magnetofossil morphology on susceptibility. Third, we quantitatively estimated the grain susceptibility of a chain of magnetosomes using B_{uni} and B_{cub}. We used the formulae from Charilaou (2017) to calculate equilibrium magnetization for 10,000 randomly oriented grains under a 0.5 mT field. Figure 10 shows the estimated susceptibility for the plausible anisotropy parameters for the equant and elongated magnetofossils. In this range, the grain susceptibility difference between the equant and elongated magnetofossils is at

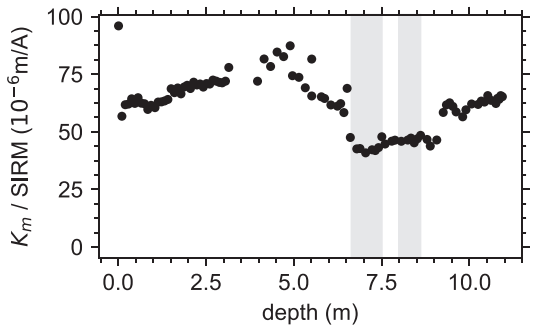

Figure 9. Depth profile of K_m / SIRM. Shaded areas indicate the intervals with the inverse AMS fabrics (6.65–7.5 and 8–8.6 m).

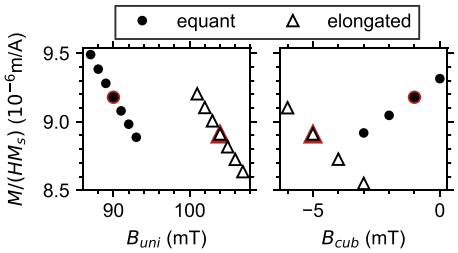

Figure 10. Estimation of grain susceptibility for the different magnetofossil morphologies for B_{uni} (left) and B_{cub} (right) constrained by the FMR data. Black circles represent the equant magnetofossils, and open triangles represent the elongated magnetofossils. Data correspond to optimal parameters estimated by FMR are highlighted by red.

most ~ 10 %, which is smaller than the variation of p in the case of $c = 0.5$ (Figure 8). Therefore, we argue that the change in AMS fabrics within the interval with near constant kARM/SIRM or M_{CR}/M_{irs} cannot be attributed to grain susceptibility, and that c is small, probably $c < 0.5$ (Figure 8). This is consistent with the small concentration of terrigenous ferrimagnetic minerals below 5.5 m (Usui et al., 2017). The value $c < 0.5$ corresponds to $p > 0.8$ (Figure 8), i.e., the magnetofossils account for > 80 % of bulk susceptibility for all sediment below 5.5 m.

The inferred high contribution of the magnetofossils to bulk susceptibility despite of the dominance of normal fabric (Figure 1) suggests lower fabric intensity of the magnetofossils than terrigenous minerals. We will examine this by modeling AMS fabrics. Noting that the AMS fabrics were mostly controlled by bedding (Figure 1), we ignore the scatter and consider one principal susceptibility closest to vertical as k_z. From the remaining two axes, k_x was chosen as the axis closer to x in core coordinates. When plotted against K_f/K_m (Figure 11), the trend of k_z was nearly linear, while k_x and k_y revealed scatter.

For samples below 5.5 m, all three values followed linear trends. Again, this may reflect different sources for the terrigenous component above 5.5 m. These results indicate that the variation of AMS fabric below 5.5 m can also be explained by the relative contribution of an inverse subfabric from ferrimagnetic minerals

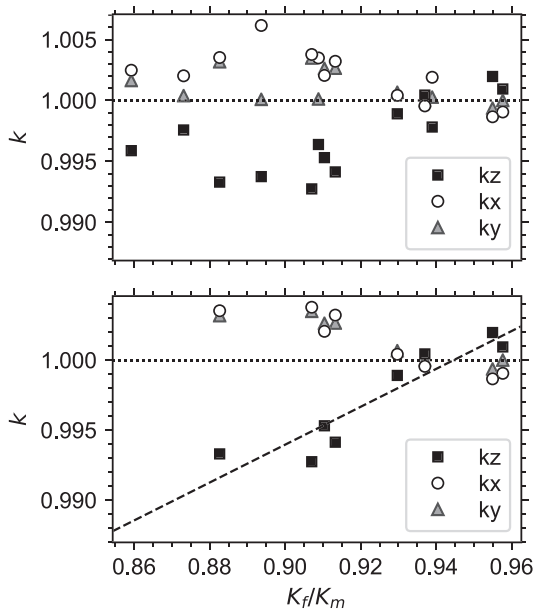

Figure 11. Normalized principal AMS versus K_f/K_m. Solid squares represent k_z, open circles k_z, and gray triangles k_y. (top) Data spanning the entire core. (bottom) Data for samples below 5.5 m. Horizontal dotted line shows $k = 1$. Dashed line in the bottom plot is a linear fit to k_z.

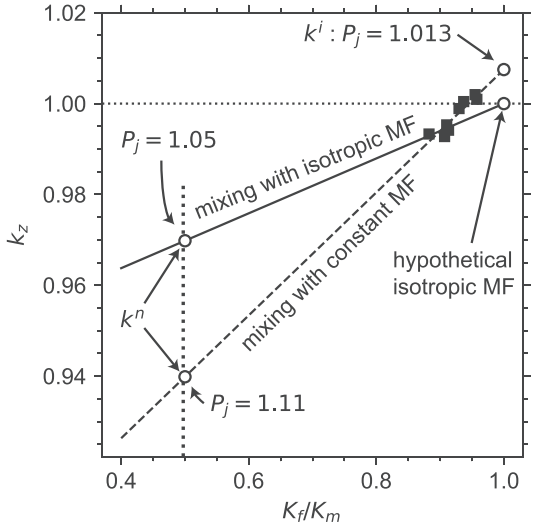

Figure 12. Graphical representation of the extrapolation to estimate the sub-fabrics. Solid squares are k_z data. Dashed line is simple extrapolation of the observed linear trend (Figure 11) which gives k^i with $P_j = 1.013$. Solid line is an extreme scenario where the fabric of magnetofossils (MF) is isotropic for K_f/K_m below the observed data (see text for more details). The normal sub-rabric k^n is found at the intersect with $K_f/K_m = c$ represented by a vertical dotted line for $c = 0.5$.

and a normal subfabric which contains fixed proportion of paramagnetic minerals as in (11). Similarly, the three-component mixing model for normalized anisotropy is

$$k = pk^i + c(1-p)k^j + (1-c)(1-p)k^p \tag{13}$$

By extrapolating the linear trend in k (Figure 11) to $K_f/K_m = 1 (p = 1)$, we can obtain an estimate of the magnetofossil subfabric (Figure 12). Approximating $K_x = K_y$, this predicts $P_j = 1.013$. This is within the typical values observed for pelagic sediment at shallow depth (Kawamura & Ogawa, 2004; Maffione & Morris, 2017). However, this comparison is not appropriate, because SD magnetite have much higher grain anisotropy compared to larger magnetite or paramagnetic minerals (Li et al., 2013; Tarling & Hrouda, 1993). By numerical calculations, Hrouda and Ježek (2017) showed that uniaxial SD magnetite requires orders of magnitude smaller preferred orientation than multidomain magnetite to achieve the same P_j of AMS. Therefore, our results indicate that the magnetofossils have much weaker sedimentary preferred orientation compared to typical pelagic sediment and that was the main reason for the limited occurrence of the inverse AMS fabric.

We can also estimate the normal subfabric by extrapolating the linear trend to lower K_f/K_m (Figure 12). In this model, ferrimagnetic normal subfabric is always present in the background, and the extrapolation is limited to $K_f/K_m = c (p = 0)$ where we would observe the pure normal subfabric $k^n = ck^j + (1-c)k^p$. We have seen that c is likely to be small (< 0.5). This predicts rather strong anisotropy; for example, a conservative value of $c = 0.5$ predicts $P_j = 1.11$ with an approximation $K_x = K_y$ (Figure 12). Similar values have been observed only for undeformed pelagic sediment obtained from >80 mbsf by ocean drillings (Kawamura & Ogawa, 2004; Maffione & Morris, 2017). We note that the assumption of constant k^i is not as safe as that for K_m^i. We have discussed that the magnitude of grain susceptibility is likely to be similar between equant and elongated magnetofossils, but we do not have evidence for similar macroscopic fabric among them. Nonetheless, even with extreme assumptions that (1) the equant magnetofossils have isotropic AMS, (2) only the equant magnetofossils are present for K_f/K_m below the observed data, and (3) $c = 0.5$, we obtain $P_j \sim 1.05$ (Figure 12). Note that this scenario reduced the anisotropy of magnetofossils, so the significant contrast in fabric intensity between magnetofossils and terrigenous minerals was not avoided. On the other hand, acoustic data suggested that > 40 m of overlying sediment is missing at the site (Nakamura et al., 2016). Therefore, we speculate that the estimated high P_j for the normal subfabric reflects the burial and subsequent erosion of significant thickness (> 80 m) of sediment. The value of c as well as k_p can be independently determined through paramagnetic anisotropy (Ferré et al., 2004; Kelso et al., 2002). Those data can test the intensity of the subfabrics. If the strong normal subfabric is special to this region, inverse AMS due to magnetofossils may be widespread among pelagic clay.

The inverse AMS fabrics clearly revealed preferred orientation of K_2 and K_3 (Figure 1). It is tempting to consider that this preferred declination reflects the alignment of magnetofossils due to the past geomagnetic field. On the other hand, it has been shown that subtle strain coming from sampling or liner deformation can induce artificial AMS (Copons et al., 1997; Shimono et al., 2014). Our data showed no clear sign of such artificial AMS (Figure 1). It is possible for magnetofossils to be more sensitive to deformation. However, the magnetofossils were estimated to have weaker sedimentary fabrics, suggesting that they may be less sensitive to the deformation due to natural compaction. The effect of the geomagnetic field on the AMS of magnetofossils may be tested by examining the reltionship with AMS and paleomagnetic directions.

7. Conclusion

Pelagic red clay from the western North Pacific revealed inverse AMS fabrics in limited intervals. Ferrimagnetic contribution dominated the mean susceptibility. Rock magnetic data indicated that the magnetofossils dominate the ferrimagnetic minerals for $\sim$ 6 m of sediment above and below the layer with the inverse fabrics, while most of the sediment showed normal AMS fabrics. Linear modeling suggested that the contribution of the magnetofossils to the mean susceptibility is likely to be > 80%. To account for the dominance of normal fabrics, the foliation of the magnetofossils must be weaker than that of terrigenous minerals. Mixing calculations for the anisotropy indicated that the magnetofossils have AMS fabrics with $P_j \sim 1.01$. Considering the high grain anisotropy of the magnetofossils, this corresponds to very weak grain foliation. AMS also suggests a preferred declination of the magnetofossils. This may reflect the past geomagnetic field direction. Alternatively, this may reflect higher sensitivity of magnetofossils to subtle artificial deformation. Mixing calculations for the anisotropy also suggested that the terrigenous minerals have strong AMS with $P_j > 1.11$. A high AMS of terrigenous minerals is consistent with the acoustic survey, suggesting erosion of > 80 m of sediment. Inverse AMS fabrics due to magnetofossils may be widespread in pelagic clay.

Acknowledgments
Data are available at Zenodo repository (doi: 10.5281/zenodo.3424949). We thank the Associate Editor Mark Dekkers and two reviewers for careful comments, which greatly improve the manuscript. This study was supported by JSPS KAKENHI Grants JP17H01361 and JP17H04855. Y. U. thanks Aguri Irisawa for assistance in the lab.

References

Bazylinski, D. A., & Frankel, R. B. (2004). Magnetosome formation in prokaryotes. *Nature Reviews Microbiology*, *2*(3), 217–230. https://doi.org/10.1038/nrmicro842

Chang, L., Harrison, R. J., Zeng, F., Berndt, T. A., Roberts, A. P., Heslop, D., & Zhao, X. (2018). Coupled microbial bloom and oxygenation decline recorded by magnetofossils during the Palaeocene-Eocene Thermal Maximum. *Nature Communications*, *9*(1), 4007. https://doi.org/10.1038/s41467-018-06472-y

Chang, L., Roberts, A. P., Winklhofer, M., Heslop, D., Dekkers, M. J., Krijgsman, W., et al. (2014). Magnetic detection and characterization of biogenic magnetic minerals: A comparison of ferromagnetic resonance and first-order reversal curve diagrams. *Journal of Geophysical Research: Solid Earth*, *119*, 6136–6158. https://doi.org/10.1002/2014JB011213

Charilaou, M. (2017). Ferromagnetic resonance of biogenic nanoparticle-chains. *Journal of Applied Physics*, *122*(6), 063903. https://doi.org/10.1063/1.4987034

Charilaou, M., Rahn-Lee, L., Kind, J., García-Rubio, I., Komeili, A., & Gehring, A. (2015). Anisotropy of bullet-shaped magnetite nanoparticles in the magnetotactic bacteria desulfovibrio magneticus sp. Strain RS-1. *Biophysical Journal*, *108*(5), 1268–1274. https://doi.org/10.1016/J.BPJ.2015.01.007

Charilaou, M., Winklhofer, M., & Gehring, A. U. (2011). Simulation of ferromagnetic resonance spectra of linear chains of magnetite nanocrystals. *Journal of Applied Physics*, *109*(9), 093903. https://doi.org/10.1063/1.3581103

Copons, R., Parés, J., Dinarès-Turell, J., & Bordonau, J. (1997). Sampling induced AMS in soft sediments: A case study in Holocene (glaciolacustrine rhythmites from Lake Barrancs (central Pyrenees, Spain). *Physics and Chemistry of the Earth*, *22*(1-2), 137–141. https://doi.org/10.1016/S0079-1946(97)00091-8

Dunlop, D. J., & Özdemir, Ö. (1997). *Rock magnetism: Fundamentals and frontiers*. Cambridge: Cambridge university press.

Egli, R. (2013). VARIFORC: An optimized protocol for calculating non-regular first-order reversal curve (FORC) diagrams. *Global and Planetary Change*, *110*, 302–320. https://doi.org/10.1016/j.gloplacha.2013.08.003

Egli, R., Chen, A. P., Winklhofer, M., Kodama, K. P., & Horng, C. S. (2010). Detection of noninteracting single domain particles using first-order reversal curve diagrams. *Geochemistry, Geophysics, Geosystems*, *11*, Q01Z11. https://doi.org/10.1029/2009GC002916

Ferré, E. C. (2002). Theoretical models of intermediate and inverse AMS fabrics. *Geophysical Research Letters*, *29*(7), 1127. https://doi.org/10.1029/2001GL014367

Ferré, E. C., Martín-Hernández, F., Teyssier, C., & Jackson, M. (2004). Paramagnetic and ferromagnetic anisotropy of magnetic susceptibility in migmatites: Measurements in high and low fields and kinematic implications. *Geophysical Journal International*, *157*(3), 1119–1129. https://doi.org/10.1111/j.1365-246X.2004.02294.x

Fischer, H., Luster, J., & Gehring, A. U. (2007). EPR evidence for maghemitization of magnetite in a tropical soil. *Geophysical Journal International*, *169*(3), 909–916. https://doi.org/10.1111/j.1365-246X.2007.03311.x

Gehring, A. U., Charilaou, M., & García-Rubio, I. (2012). Oxidized magnetosomes in magnetotactic bacteria. *Journal of Magnetism and Magnetic Materials*, *324*(7), 1281–1284. https://doi.org/10.1016/j.jmmm.2011.10.039

Gehring, A. U., Kind, J., Charilaou, M., & García-Rubio, I. (2011). The detection of magnetotactic bacteria and magnetofossils by means of magnetic anisotropy. *Earth and Planetary Science Letters*, *309*(1-2), 113–117. https://doi.org/10.1016/j.epsl.2011.06.024

Girdler, R. W. (1961). The measurement and computation of anisotropy of magnetic susceptibility of rocks. *Geophysical Journal International*, *5*(1), 34–44. https://doi.org/10.1111/j.1365-246X.1961.tb02927.x

Henry, B., & Daly, L. (1983). From qualitative to quantitative magnetic anisotropy analysis: The prospect of finite strain calibration. *Tectonophysics*, *98*(3-4), 327–336. https://doi.org/10.1016/0040-1951(83)90300-1

Heslop, D., Roberts, A. P., Chang, L., Davies, M., Abrajevitch, A., & De Deckker, P. (2013). Quantifying magnetite magnetofossil contributions to sedimentary magnetizations. *Earth and Planetary Science Letters*, *382*, 58–65. https://doi.org/10.1016/j.epsl.2013.09.011

Hesse, P. P. (1994). Evidence for bacterial palaeoecological origin of mineral magnetic cycles in oxic and sub-oxic Tasman Sea sediments. *Marine Geology*, *117*(1-4), 1–17. https://doi.org/10.1016/0025-3227(94)90003-5

Hrouda, F., & Ježek, J. (2017). Role of single-domain magnetic particles in creation of inverse magnetic fabrics in volcanic rocks: A mathematical model study. *Studia Geophysica et Geodaetica*, *61*(1), 145–161. https://doi.org/10.1007/s11200-015-0675-6

Jackson, M. (1991). Anisotropy of magnetic remanence: A brief review of mineralogical sources, physical origins, and geological applications, and comparison with susceptibility anisotropy. *Pure and Applied Geophysics*, *136*(1), 1–28. https://doi.org/10.1007/BF00878885

Jackson, M., & Tauxe, L. (1991). Anisotropy of magnetic susceptibility and remanence: Developments in the characterization of tectonic, sedimentary and igneous fabric. *Reviews of Geophysics*, *29*(S1), 371–376. https://doi.org/10.1002/rog.1991.29.s1.371

Jelinek, V. (1981). Characterization of the magnetic fabric of rocks. *Tectonophysics*, *79*(3-4), T63–T67. https://doi.org/10.1016/0040-1951(81)90110-4

Just, J., Dekkers, M. J., von Dobeneck, T., van Hoesel, A., & Bickert, T. (2012). Signatures and significance of aeolian, fluvial, bacterial and diagenetic magnetic mineral fractions in Late Quaternary marine sediments off Gambia, NW Africa. *Geochemistry, Geophysics, Geosystems*, *13*, Q0AO02. https://doi.org/10.1029/2012GC004146

Kanamatsu, T., Parés, J. M., & Kitamura, Y. (2012). Pliocene shortening direction in Nankai Trough off Kumano, southwest Japan, Sites IODP C0001 and C0002, Expedition 315: Anisotropy of magnetic susceptibility analysis for paleostress. *Geochemistry, Geophysics, Geosystems*, *13*, Q0AD22. https://doi.org/10.1029/2011GC003782

Kawamura, K., & Ogawa, Y. (2004). Progressive change of pelagic clay microstructure during burial process: Examples from piston cores and ODP cores. *Marine Geology*, *207*(1-4), 131–144. https://doi.org/10.1016/J.MARGEO.2004.03.016

Kelso, P. R., Tikoff, B., Jackson, M., & Sun, W. (2002). A new method for the separation of paramagnetic and ferromagnetic susceptibility anisotropy using low field and high field methods. *Geophysical Journal International*, *151*(2), 345–359. https://doi.org/10.1046/j.1365-246X.2002.01732.x

Kirschvink, J. L., & Chang, S. R. (1984). Ultrafine-grained magnetite in deep-sea sediments: Possible bacterial magnetofossils. *Geology*, *12*(9), 559–562. https://doi.org/10.1130/0091-7613 (1984)12<559:UMIDSP>2.0.CO;2

Kon, S., Nakamura, N., Nishimura, Y., Goto, K., & Sugawara, D. (2017). Inverse magnetic fabric in unconsolidated sandy event deposits in Kiritappu Marsh, Hokkaido, Japan. *Sedimentary Geology*, *349*, 112–119. https://doi.org/10.1016/J.SEDGEO.2017.01.003

Kopp, R. E., Raub, T. D., Schumann, D., Vali, H., Smirnov, A. V., & Kirschvink, J. L. (2007). Magnetofossil spike during the Paleocene-Eocene thermal maximum: Ferromagnetic resonance, rock magnetic, and electron microscopy evidence from Ancora, New Jersey, United States. *Paleoceanography*, *22*, PA4103. https://doi.org/10.1029/2007PA001473

Kopp, R. E., Weiss, B. P., Maloof, A. C., Vali, H., Nash, C. Z., & Kirschvink, J. L. (2006). Chains, clumps, and strings: Magnetofossil taphonomy with ferromagnetic resonance spectroscopy. *Earth and Planetary Science Letters*, *247*(1-2), 10–25. https://doi.org/10.1016/j.epsl.2006.05.001

Lanci, L. (2010). Detection of multi-axial magnetite by remanence effect on anisotropy of magnetic susceptibility. *Geophysical Journal International*, *181*(3), 1362–1366. https://doi.org/10.1111/j.1365-246X.2010.04588.x

Lanci, L., & Zanella, E. (2016). The anisotropy of magnetic susceptibility of uniaxial superparamagnetic particles: Consequences for its interpretation in magnetite and maghemite bearing rocks. *Journal of Geophysical Research: Solid Earth*, *121*, 27–37. https://doi.org/10.1002/2015JB012255

Lascu, I., Harrison, R. J., Li, Y., Muraszko, J. R., Channell, J. E. T., Piotrowski, A. M., & Hodell, D. A. (2015). Magnetic unmixing of first-order reversal curve diagrams using principal component analysis. *Geochemistry, Geophysics, Geosystems*, *16*, 2900–2915. https://doi.org/10.1002/2015GC005909

Lefèvre, C. T., Pósfai, M., Abreu, F., Lins, U., Frankel, R. B., & Bazylinski, D. A. (2011). Morphological features of elongated-anisotropic magnetosome crystals in magnetotactic bacteria of the Nitrospirae phylum and the Deltaproteobacteria class. *Earth and Planetary Science Letters*, *312*(1-2), 194–200. https://doi.org/10.1016/j.epsl.2011.10.003

Li, J., Ge, K., Pan, Y., Williams, W., Liu, Q., & Qin, H. (2013). A strong angular dependence of magnetic properties of magnetosome chains: Implications for rock magnetism and paleomagnetism. *Geochemistry, Geophysics, Geosystems*, *14*, 3887–3907. https://doi.org/10.1002/ggge.20228

Li, J., Wu, W., Liu, Q., & Pan, Y. (2012). Magnetic anisotropy, magnetostatic interactions and identification of magnetofossils. *Geochemistry, Geophysics, Geosystems*, *13*, Q10Z51. https://doi.org/10.1029/2012GC004384

MacDonald, W. D., & Ellwood, B. B. (1987). Anisotropy of magnetic susceptibility: Sedimentological, igneous, and structural-tectonic applications. *Reviews of Geophysics*, *25*(5), 905–909. https://doi.org/10.1029/RG025i005p00905

Maffione, M., & Morris, A. (2017). The onset of fabric development in deep marine sediments. *Earth and Planetary Science Letters*, *474*, 32–39. https://doi.org/10.1016/J.EPSL.2017.06.018

Mao, X., Egli, R., Petersen, N., Hanzlik, M., & Zhao, X. (2014). Magnetotaxis and acquisition of detrital remanent magnetization by magnetotactic bacteria in natural sediment: First experimental results and theory. *Geochemistry, Geophysics, Geosystems*, *15*, 255–283. https://doi.org/10.1002/2013GC005034@10.1002/(ISSN)1525-2027.ATOMIC2

Nakamura, K., Machida, S., Okino, K., Masaki, Y., Iijima, K., Suzuki, K., & Kato, Y. (2016). Acoustic characterization of pelagic sediments using sub-bottom profiler data: Implications for the distribution of REY-rich mud in the Minamitorishima EEZ, western Pacific. *Geochemical Journal*, *50*(6), 605–619. https://doi.org/10.2343/geochemj.2.0433

Pósfai, M., Moskowitz, B. M., Arató, B., Schüler, D., Flies, C., Bazylinski, D. A., & Frankel, R. B. (2006). Properties of intracellular magnetite crystals produced by Desulfovibrio magneticus strain RS-1. *Earth and Planetary Science Letters*, *249*(3-4), 444–455. https://doi.org/10.1016/J.EPSL.2006.06.036

Parés, J., Hassold, N., Rea, D., & van der Pluijm, B. (2007). Paleocurrent directions from paleomagnetic reorientation of magnetic fabrics in deep-sea sediments at the Antarctic Peninsula Pacific margin (ODP Sites 1095, 1101). *Marine Geology*, *242*(4), 261–269. https://doi.org/10.1016/J.MARGEO.2007.04.002

Petersen, N., von Dobeneck, T., & Vali, H. (1986). Fossil bacterial magnetite in deep-sea sediments from the South Atlantic Ocean. *Nature*, *6063*, 611–615. https://doi.org/10.1038/320611a0

Potter, D. K., & Stephenson, A. (1988). Single-domain particles in rocks and magnetic fabric analysis. *Geophysical Research Letters*, *15*(10), 1097–1100. https://doi.org/10.1029/GL015i010p01097

Roberts, A. P., Chang, L., Heslop, D., Florindo, F., & Larrasoaña, J. C. (2012). Searching for single domain magnetite in the "pseudo-single-domain" sedimentary haystack: Implications of biogenic magnetite preservation for sediment magnetism and relative paleointensity determinations. *Journal of Geophysical Research*, *117*, B08104. https://doi.org/10.1029/2012JB009412

Roberts, A. P., Florindo, F., Chang, L., Heslop, D., Jovane, L., & Larrasoaña, J. C. (2013). Magnetic properties of pelagic marine carbonates. *Earth-Science Reviews*, *127*, 111–139. https://doi.org/10.1016/j.earscirev.2013.09.009

Roberts, A. P., Florindo, F., Villa, G., Chang, L., Jovane, L., Bohaty, S. M., et al. (2011). Magnetotactic bacterial abundance in pelagic marine environments is limited by organic carbon flux and availability of dissolved iron. *Earth and Planetary Science Letters*, *310*(3-4), 441–452. https://doi.org/10.1016/j.epsl.2011.08.011

Rochette, P., Jackson, M., & Aubourg, C. (1992). Rock magnetism and the interpretation of anisotropy of magnetic susceptibility. *Reviews of Geophysics*, *30*(3), 209. https://doi.org/10.1029/92RG00733

Schwehr, K., Tauxe, L., Driscoll, N., & Lee, H. (2006). Detecting compaction disequilibrium with anisotropy of magnetic susceptibility. *Geochemistry, Geophysics, Geosystems*, *7*, Q11002. https://doi.org/10.1029/2006GC001378

Shimono, T., & Yamazaki, T. (2016). Environmental rock-magnetism of Cenozoic red clay in the South Pacific Gyre. *Geochemistry, Geophysics, Geosystems*, *17*, 1296–1311. https://doi.org/10.1002/2015GC006062

Shimono, T., Yamazaki, T., & Inoue, S. (2014). Influence of sampling on magnetic susceptibility anisotropy of soft sediments: Comparison between gravity and piston cores. *Earth, Planets and Space*, *66*(1), 3. https://doi.org/10.1186/1880-5981-66-3

Tarling, D., & Hrouda, F. (1993). The magnetic anisotropy of rocks.

Usui, Y., Yamazaki, T., & Saitoh, M. (2017). Changing abundance of magneto fossil morphologies in pelagic red clay around minamitorishima, western North Pacific. *Geochemistry, Geophysics, Geosystems*, *18*, 4558–4572. https://doi.org/10.1002/2017GC007127

von Dobeneck, T. (1996). A systematic analysis of natural magnetic mineral assemblages based on modelling hysteresis loops with coercivity-related hyperbolic basis functions. *Geophysical Journal International*, *124*(3), 675–694. https://doi.org/10.1111/j.1365-246X.1996.tb05632.x

Weiss, B. P., Sam Kim, S., Kirschvink, J. L., Kopp, R. E., Sankaran, M., Kobayashi, A., & Komeili, A. (2004). Ferromagnetic resonance and low-temperature magnetic tests for biogenic magnetite. *Earth and Planetary Science Letters*, *224*(1-2), 73–89. https://doi.org/10.1016/j.epsl.2004.04.024

Yamazaki, T. (2012). Paleoposition of the Intertropical Convergence Zone in the eastern pacific inferred from glacial-interglacial changes in terrigenous and biogenic magnetic mineral fractions. *Geology*, *40*(2), 151–154. https://doi.org/10.1130/G32646.1

Yamazaki, T., & Kawahata, H. (1998). Organic carbon flux controls the morphology of magnetofossils in marine sediments. *Geology*, *26*(12), 1064–1066. https://doi.org/10.1130/0091-7613 (1998)026<1064:OCFCTM>2.3.CO;2

Yamazaki, T., & Shimono, T. (2013). Abundant bacterial magnetite occurrence in oxic red clay. *Geology*, *41*(11), 1191–1194. https://doi.org/10.1130/G34782.1

Yamazaki, T., Suzuki, Y., Kouduka, M., & Kawamura, N. (2019). Dependence of bacterial magnetosome morphology on chemical conditions in deep-sea sediments. *Earth and Planetary Science Letters*, *513*, 135–143. https://doi.org/10.1016/J.EPSL.2019.02.015